

Tip-Enhanced Strong-Field Photoemission

R. Bormann, M. Gulde, A. Weismann, S. V. Yalunin, and C. Ropers*

Courant Research Center Nano-Spectroscopy and X-Ray Imaging, University of Göttingen, 37077 Göttingen, Germany
(Received 26 May 2010; revised manuscript received 13 August 2010; published 27 September 2010)

Nonlinear photoelectron emission from metallic nanotips is explored in the strong-field regime. The passage between the multiphoton and the optical field emission regimes is clearly identified. The experimental observations are in agreement with a quantum mechanical strong-field model.

DOI: 10.1103/PhysRevLett.105.147601

PACS numbers: 79.60.Jv, 42.65.Re, 73.20.Mf

Single- and multiphoton photoemission spectroscopy from solids are powerful tools to map electronic band structures [1] and follow excited electron dynamics [2], respectively. The physics behind these techniques is based on linear and low order nonlinear interactions of light with bound electrons. In contrast, *strong-field* photoelectron emission—where “strong” refers to the dominance of the optical fields over the binding fields—has proven much less accessible than its counterpart in atomic and molecular gases [3–5], mainly because of optical damage thresholds and space charge effects at high carrier densities. Nonetheless, from the discoveries in atomic strong-field ionization leading to attosecond science [6], very rich behavior is expected upon extending photoemission from solids into the strong-field regime.

Ultrafast, localized photoemission from nanostructures is of particular interest, partly because of its potential for enhancing time-resolved electron microscopy [7] and diffraction [8], and use in single-electron sources or carrier envelope phase detection [9–11]. Ultrafast electron sources of great spatial coherence combine optical field enhancements at metal nanotips with nonlinear photoelectric effects [12,13]. Recently, localized electron emission from such structures was induced with low-energy femtosecond pulses [11–17]. The underlying emission processes responsible for the observations have—for the nonlinear case—been controversially discussed in terms of multiphoton electron emission (perturbative regime) [12,14–16] or optical field emission [11,13]. Recently, damage thresholds were found to limit intensities to the multiphoton regime for tungsten tips [16]. These issues are of significant importance, both from the fundamental perspective of understanding strong-field effects in solids and because emission by optical tunneling with ultrashort pulses may ultimately result in electron timing precisions of the optical half-cycle or less.

Here, we present a study of strong-field photoelectron emission from single metal nanostructures. The transition between multiphoton photoemission and optical field emission is resolved. Space charge disturbance or inhomogeneous field distributions do not obscure these observations, as evidenced by both the intensity dependence of the electron current and the spatial emission characteristics.

A quantum mechanical model using a strong-field approximation (SFA) agrees with the measurements.

Nanostructures, specifically sharp metallic tips, possess unique assets for the study of nonlinear phenomena at high intensities. In the case of studying an individual nanotip with a single optical “hot spot” at its apex, the locally amplified intensity is very well defined and will display no stochastic spread of field enhancement values, as found at an imperfect or rough planar surface. This allows one to controllably approach the local damage threshold. Gold structures, with plasmon-induced intensity enhancements of at least 2 orders of magnitude, make nonlinear optical effects observable at low incident powers and high pulse repetition rates [12,18–20]. However, under these conditions, the peak intensities that avoid structural damage are often limited by the incident time-averaged power rather than the single pulse damage threshold, so that lower repetition rates allow for studying these processes at higher peak intensities [16].

Thus, in the present experiments, we employ ultrashort laser pulses at a low rate. Pulses from a Ti:Sapphire amplifier (duration 30 fs, center wavelength 830 nm, repetition rate 1 kHz) are focused by a Schwarzschild objective (2.5 μm focus diameter) onto an electrochemically etched gold tip (about 20 nm apex radius) in an ultrahigh-vacuum chamber [cf. Fig. 1]. The polarization is parallel to the tip axis. Moderate negative bias voltages (typically 10–30 V) are applied to the tip. Variable attenuation is provided by a

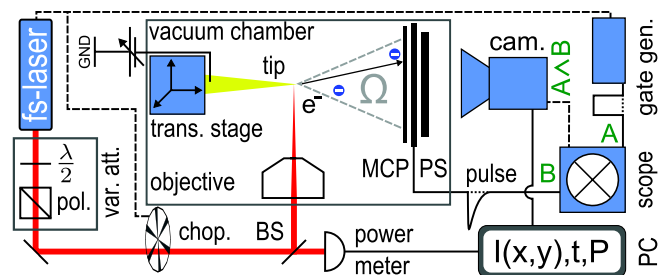


FIG. 1 (color online). Experimental setup. Laser pulses are focused onto a gold tip in a vacuum chamber. Electrons are detected and imaged by microchannel plates (MCP) and a CCD camera. t : electron arrival time. P : laser power. BS: beam splitter. PS: phosphor screen. $I(x, y)$: CCD image.

half-wave plate and polarizer, and the number of electrons emitted for every laser pulse is measured by a microchannel plate with phosphor screen, read out both electronically and by a timed and triggered charge-coupled device (CCD) camera. For single pulse images, the repetition rate is reduced to 100 Hz by a mechanical chopper. A computer routine finding local maxima in the CCD image counts up to thousands of electrons per image with less than 5% error.

Figure 2(a) displays the electron current versus incident pulse energy on a double-logarithmic scale (circles), and typical single-shot CCD images. Previous measurements on similar gold tips reported emission rates up to about 0.1 per laser pulse [12], roughly corresponding to the experimental conditions at the lower ends of the graph. Here, at the highest pulse energies, more than 1000 electrons per pulse are detected.

At low count rates, a strongly nonlinear pulse energy (and corresponding intensity) dependence is observed, which approximately follows the fifth-order power law (dashed line) of a multiphoton process. Around 0.6 nJ, i.e., at an incident peak intensity of about 4×10^{11} W/cm², the curve departs this behavior, and a relatively abrupt transition to a lower (again nearly uniform) power law dependence is found. The intensity dependent slope of the curve [cf. Fig. 2(b) (squares)] illustrates the transition.

The spatially resolved CCD images are used to extract the solid angle Ω , into which the emission occurs. It is defined by the full-widths D_x , D_y of the distributions of events, and the tip-detector distance d : $\Omega = \pi D_x D_y / 4d^2$. Interestingly, the transition in intensity dependence is

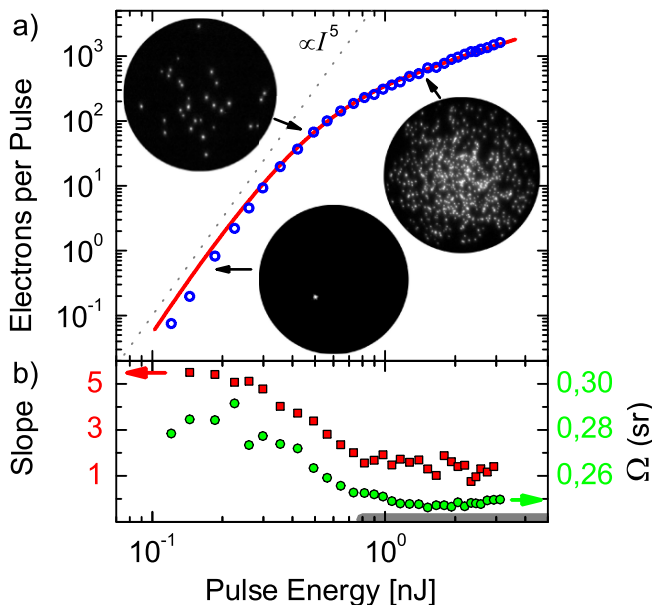


FIG. 2 (color online). (a) Pulse energy dependence of electron current (circles), fifth-order power law (dotted grey) and SFA model [solid (red)]. Insets: single-shot images. (b) Pulse energy dependence of effective nonlinearity [slope of curve in (a), (red) squares] and solid angle of emission [(green) circles].

paralleled by a change of Ω [cf. Fig. 2(b), light grey (green) circles]. In fact, the solid angle of the emission approaches that found for a 15 V higher static bias at low intensities [cf. Fig. 2(b), gray line in bottom], before it rises slowly at pulse energies above 2 nJ.

Very similar results on several tips (at varying transition energies) indicate that tip damage is usually avoided for energies up to a factor of 6 above the kink in nonlinearity. The emission current in Fig. 2 is reproduced in scanning the range of incident energies 10 times, ruling out tip damage during this measurement. In contrast, recent low-repetition-rate experiments on tungsten tips found that damage occurs near an emission close to 10 electrons per pulse, and without a noticeable deviation from multiphoton behavior [16]. In the present study, the lower optical absorption of gold allows for the application of much higher local intensities.

The emission at low intensities is proportional to the fifth power of the intensity, while the work function (~ 5 eV) requires only four photons for photoemission. In fact, for blunter tips, we have in some cases found four-photon nonlinearities. Previous photoemission computations [9] and experiments on plane surfaces [21] have identified similar increases, but with differing interpretations. Here, besides possible geometrical effects, an enhanced contribution from the large density of d -band initial states about 2 eV below the Fermi energy may contribute to enhanced nonlinearities. Inspection of gold's band structure indicates a sharp increase of the joint density of states for total transition energies above 6.5 eV. These open questions will be the subject of further study.

Interpreting the observed reduction of nonlinearity at high count rates warrants special care because not only strong-field emission—as we will show—but also other factors, such as detector nonlinearities and especially space charge effects, may lead to various forms of saturation behavior. Detector saturation was ruled out in reference measurements. Space charge saturation is a well-known problem in multiphoton photoemission from planar surfaces [4,21,22], particularly at longer pulse durations, but has usually been found at substantially lower values of both fluence and current density. Thus, it is evident that the tip geometry, with radially diverging particle trajectories and large static (lightning rod) field enhancement for rapid charge acceleration, is less susceptible to space charge than a planar surface. Furthermore, whereas space charge is expected to result in an increase of the transverse spread of the electron bunch, the opposite, namely, a reduced emission solid angle, is found for high intensities. A weak increase of Ω , and perhaps the onset of space charge broadening, is only observed at the highest count rates. Hence, the solid angle reduction suggests that the transition in intensity dependence is not primarily associated with space charge. Rather, the behavior indicates a transfer of forward momentum from the laser field to the electrons in the direction of light polarization, which is a hallmark of

strong-field conditions, in which the electron kinetic energy is significantly influenced by the interaction with the laser field [6,23]. Such behavior was in fact predicted theoretically for plasmon-assisted photoelectron generation [24].

The transition between multiphoton emission and high-order optical field emission is characterized in terms of the Keldysh parameter $\gamma = \sqrt{I_0/(2U_{\text{pon}})}$, where I_0 is the ionization energy (or work function) and $U_{\text{pon}} = E^2/(4\omega^2)$ is the ponderomotive energy (in atomic units), which is the average kinetic energy of an electron in an oscillating field of strength E at frequency ω [23]. The multiphoton regime ($\gamma \gg 1$) is governed by the absorption of well-defined (small) integer numbers of photons, while in optical field emission ($\gamma \ll 1$), multiple processes of high photon numbers contribute.

In order to obtain a single description covering both the weak- and strong-field regimes, we model the photoemission in the framework of time-dependent perturbation theory using a SFA [23]. The optical field induces electric dipole transitions from initial states $|\psi_i\rangle$ with energy ϵ_i at the metal surface into a set of final Volkov states $|\psi_f\rangle$ [25]. These final states are solutions to the time-dependent Schrödinger equation in a spatially linear, time-harmonic potential. In essence, Volkov states are time-dependent plane waves, whose momentary energy consists of a harmonically time-varying component (due to quiver motion) superimposed on a drift motion with momentum p . The light-induced scalar potential V_L , in which transitions are considered, is linearly varying in the vacuum and exponentially decaying into the solid with optical decay length l . A tip-geometry-induced spatial dependence in a vacuum is ignored, since the wave function decay length of the initial states into a vacuum is much shorter than the tip radius. Thus, we assume $V_L = Eb \exp(z/l) \cos(\omega t)$ for $z < 0$ and $V_L = -E(z-b) \cos(\omega t)$ for $z \geq 0$ with a constant $b = l/\epsilon$ (ϵ : metal permittivity). Since the perturbation theory is not strictly gauge independent [26], this choice of b corresponds to selecting a suitable gauge for delocalized initial states (decaying perturbation in the solid). The SFA implies that the initial states are treated as unperturbed by the laser field, while the final states are unperturbed by the binding potential of the solid (including image charges).

In a harmonic field, the possible transitions are characterized by the absorption of integer numbers of photons n . For a given n , the transition rate can be written in terms of an integral over the light period T , i.e., $D_n(E, \epsilon_i) = 2\pi |T^{-1} \int V_{L,if} dt|^2 g_v(\epsilon_f)$, where $V_{L,if} = \langle \psi_i | V_L | \psi_f \rangle$ and $g_v(\epsilon_f)$ is the (3D) vacuum density of states at the final energy. The total emission rate per unit area and time is then given as a sum over all transition channels: $\Gamma(E, \epsilon_i) = \sum_n D_n(E, \epsilon_i)$. We restrict these computations to direct (single-step) multiphoton transitions and exclude step-wise excitations, which would involve a more in-depth treatment of band structure and dephasing, which is beyond the scope of the present work.

The initial states belonging to the solid band structure are taken exponentially decaying with constant $\alpha = \sqrt{-2\epsilon_i}$ into the vacuum (energy zero is taken as the vacuum level). The final states are Volkov states [25] with momentum p and energy $\epsilon_f = p^2/2 + U_{\text{pon}}$. The momentum p is the time-averaged momentum, with which the Volkov solution propagates. The spatial part of the integration in the matrix element can readily be performed. We consider presently only contributions to the matrix elements in the vacuum half space, first because the field in the solid is reduced by a factor $|\epsilon|$, which will greatly suppress contributions nonlinearly varying in the field. Second, the used final states are only defined in vacuum, and there is no simple extension of the approach to states solving the Schrödinger equation including the boundary. With these considerations, $T^{-1} \int V_{L,if} dt$ reduces to

$$\begin{aligned} & \int_0^{2\pi} d\phi \rho(\phi) \exp[iS(\phi)] \\ & \doteq \int_0^{2\pi} d\phi \left[1 - i\frac{p}{\alpha} - i\frac{E}{\alpha\omega} \sin(\phi) \right] \\ & \cdot \exp \left[in\phi - i\frac{pE}{\omega^2} \cos(\phi) - i\frac{E^2}{8\omega^3} \sin(2\phi) \right. \\ & \left. + i\frac{Eb}{\omega} \sin(\phi) \right], \end{aligned}$$

with real ρ and S , which is evaluated numerically.

Figure 3(a) shows the transition rates of different channels [grey (colored) lines] and the sum over all channels (black line) as a function of γ . The individual contributions of the channels labeled by n correspond to the different multiphoton orders and grow with the n th power of the intensity ($\propto \gamma^{-2}$) at low intensities, before they begin oscillating and drop to zero [23]. The physical meaning of this cutoff lies in the fact that the quiver motion of the emitted electron poses an additional contribution to the final state energy (in the form of the ponderomotive potential proportional to intensity), which must be supplied by the absorption of the given number of n photons for any channel. From $p = \sqrt{2(\epsilon_i + n\omega - U_{\text{pon}})}$, it is clear that for every channel number n , there is a maximum field strength, at which p is real, so that the Volkov state is propagating. This channel-closing of any multiphoton order is well known in atomic strong-field ionization.

The sum over all channels displays a transition from a steep slope at low intensities, where only the lowest order channels contribute, towards a smaller slope at intensities, where many channels of high n contribute. In the case of atomic ionization, similar kinks are attributed to a combination of saturation and an enhancement of the active ionization volume [27]. In our case, however, a significant increase in this volume would appear as an increase in Ω , which is, as previously noted, not observed. In the present perturbative model, the relatively abrupt transition depends on the size of the field penetration parameter b , which

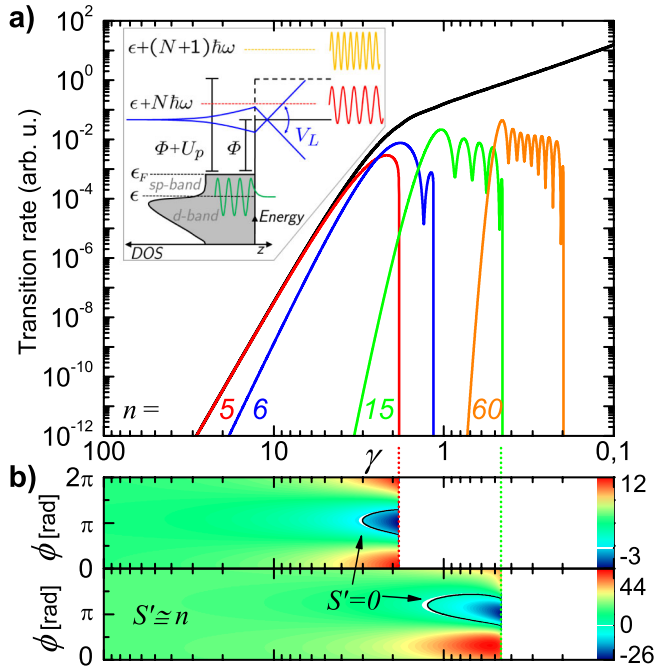


FIG. 3 (color online). Results of the model computations. (a) Transition rate for single channels [grey (color)] and total sum (solid black) ($\epsilon_i = -4.3\omega$) as a function of Keldysh parameter. Inset: Schematic of the model. (b) S' (see text) for $n = 5$ (top panel) and $n = 15$ (bottom panel).

accounts for the energy gained by the delocalized initial state in the metal. In numerical integrations of the Schrödinger equation, which will be presented in detail elsewhere, we have found a very similar behavior and slope changes for delocalized initial states.

Despite its approximations and shortcomings, the model rather accurately reproduces the experiments. With an electric field enhancement of about 8, which conforms with previous findings for such tips [12], and $\epsilon_i = -4.3\omega$ (accounting for the increased initial slope), very good agreement with the measurements is obtained [solid (red) line in Fig. 2]. For this comparison, the number of emitted electrons per pulse is obtained by integration over the electric field envelope of the pulse (implying a slowly varying envelope approximation) and the apex area. For simplicity, the initial states are normalized to yield the experimental five-photon cross section [in terms of current per unit area and local (enhanced) intensity] at weak fields, $\sigma_5 \approx 10^{-71} \text{ A nm}^{-2} \text{ cm}^{10} \text{ W}^{-5}$. At the transition, predicted by the model near $\gamma \approx 2$, local peak intensities of greater than 10^{13} W/cm^2 then occur at the apex, not resulting in permanent damage. It has been shown that similar intensities at nanostructures are achieved in plasmon-enhanced high-harmonic generation [18].

Finally, let us briefly consider the observed oscillations in the individual channel contributions. They are understood by analyzing the angular derivative of the phase of the integrand discussed above, which is closely related to the quantum mechanical action of the process $S' \doteq \frac{dS}{d\phi}$.

Figure 3(b) displays S' in color scale for two channels as a function of γ and phase. Near the transition to the strong-field regime, stationary phase points (i.e., two near-classical trajectories with $S' = 0$) arise. These interfere, much like long and short paths in high-harmonic generation [6], leading to the oscillatory matrix elements.

In summary, we have presented results on highly nonlinear photoemission from single metal nanotips beyond the multiphoton regime, which are successfully described in terms of a perturbation treatment using a strong-field approximation. We expect that investigations of the kinetic energies of the emitted electrons and carrier envelope phase effects will further expand strong-field interactions into the domain of nanostructures and interfaces.

We thank W. Becker and D. R. Solli for useful discussions. Support by the Deutsche Forschungsgemeinschaft (DFG-ZUK 45/1 and SPP 1391) and EU Erasmus Mundus is gratefully acknowledged.

*croppers@gwdg.de

- [1] S. Hüfner, *Photoelectron Spectroscopy: Principles and Applications* (Springer, Berlin, 2003).
- [2] H. Petek and S. Ogawa, *Prog. Surf. Sci.* **56**, 239 (1997).
- [3] Gy. Farkas, Z. Gy. Horváth, and I. Kertész, *Phys. Lett. A* **39**, 231 (1972).
- [4] M. Aeschlimann *et al.*, *J. Chem. Phys.* **102**, 8606 (1995).
- [5] G. Ferrini, F. Banfi, C. Giannetti, and F. Parmigiani, *Nucl. Instrum. Methods Phys. Res., Sect. A* **601**, 123 (2009).
- [6] F. Krausz and M. Ivanov, *Rev. Mod. Phys.* **81**, 163 (2009).
- [7] J. S. Kim *et al.*, *Science* **321**, 1472 (2008).
- [8] B. J. Siwick *et al.*, *Science* **302**, 1382 (2003).
- [9] C. Lemell, X.-M. Tong, F. Krausz, and J. Burgdörfer, *Phys. Rev. Lett.* **90**, 076403 (2003).
- [10] A. Apolonski *et al.*, *Phys. Rev. Lett.* **92**, 073902 (2004).
- [11] P. Hommelhoff, C. Kealhofer, and M. A. Kasevich, *Phys. Rev. Lett.* **97**, 247402 (2006).
- [12] C. Ropers *et al.*, *Phys. Rev. Lett.* **98**, 043907 (2007).
- [13] P. Hommelhoff *et al.*, *Phys. Rev. Lett.* **96**, 077401 (2006).
- [14] C. Ropers *et al.*, *New J. Phys.* **9**, 397 (2007).
- [15] B. Barwick *et al.*, *New J. Phys.* **9**, 142 (2007).
- [16] S. A. Hilbert *et al.*, *J. Phys. B* **42**, 141001 (2009).
- [17] H. Yanagisawa *et al.*, *Phys. Rev. Lett.* **103**, 257603 (2009).
- [18] S. Kim *et al.*, *Nature (London)* **453**, 757 (2008).
- [19] A. Bouhelier *et al.*, *Phys. Rev. Lett.* **90**, 013903 (2003).
- [20] S. E. Irvine, A. Dechant, and A. Y. Elezzabi, *Phys. Rev. Lett.* **93**, 184801 (2004).
- [21] J. G. Fujimoto, J. M. Liu, E. P. Ippen, and N. Bloembergen, *Phys. Rev. Lett.* **53**, 1837 (1984).
- [22] P. Muggli, R. Brogle, and C. Joshi, *J. Opt. Soc. Am. B* **12**, 553 (1995).
- [23] H. R. Reiss, *Phys. Rev. A* **22**, 1786 (1980).
- [24] P. Dombi and P. Rác, *Opt. Express* **16**, 2887 (2008).
- [25] D. M. Volkov, *Z. Phys.* **94**, 250 (1935).
- [26] D. Bauer, D. B. Milošević, and W. Becker, *Phys. Rev. A* **72**, 023415 (2005).
- [27] A. Becker, F. H. M. Faisal, *Phys. Rev. A* **59**, R1742 (1999).